JOURNAL OF MATERIALS SCIENCE **39** (2004) 413–431

Morphology-tensile behavior relationship in injection molded poly(ethylene terephthalate)/polyethylene and polycarbonate/polyethylene blends (I)

Part I *Skin-core structure*

ZHONG-MING LI, WEI YANG
College of Polymer Science and Engineering, State Key Laboratory of Polymer Materials Engineering, Sichuan University, Chengdu, 610065, Sichuan, People's Republic of China

SHUYING YANG
Mechanical Engineering Department, University of Texas Pan America, Edinburg, TX 78541, USA

RUI HUANG, MING-BO YANG*
College of Polymer Science and Engineering, State Key Laboratory of Polymer Materials Engineering, Sichuan University, Chengdu, 610065, Sichuan, People's Republic of China
E-mail: yangmb@scu.edu.cn

The skin-core structure of injection molded poly(ethylene terephthalate) (PET)/polyethylene (PE) and polycarbonate (PC)/PE blends was investigated. The results indicate that both shape and size of the PET and PC phases depended not only on the nature properties of PET/PE and PC/PE blends, but also on the injection molding parameters such as injection speed and the positions in the molded bars. The morphology in the section perpendicular to the melt flow direction included four layers, surface, sub-skin, intermediate layers as well as core zone. The surface layer was ignored in the present study. The sub-skin layer contained more or less fibrous structure and its thickness gradually decreased along the molded bar from the gate toward the non-gate end. At the same injection speed, the concentration of the injection-induced fibers in PC/PE blend was much higher than that in PET/PE blend. In the core region, the dispersed phase was mainly composed of spherical particles whose diameter increased along the melt flow pathway. Between these two layers, there was an intermediate layer where the dispersed particles mainly assumed the form of fibers, ellipsoids or spheres. Generally, no matter whether the dispersed particles were elongated or not during injection molding, the PET particles were larger than PC ones.

1. Introduction

Immiscible blends form a multi-system with a deformable minor phase which, under appropriate conditions, could be deformed *in situ* into morphological structures such as spheres, ellipsoids, fibers, and plates or ribbons during melt processing [1–3]. A part made from a polymer blend generally experiences two melt processing stages: blend fabrication and subsequent part production. Both stages play an important role in formation of the final blend morphology [4–8]. It is well known that, during melt processing, several factors are particularly important in determining the final size and shape of the dispersed phase: composition, interfacial tension, time of mixing, shear rate or shear stress, elasticity of the components and viscosity ratio (ratio of viscosity of the dispersed phase to that of the matrix) [9, 10]. The influences of these parameters on the morphology of blends in various melt mixing operations of original polymer resins, e.g., internal mixer, single-/twin-screw extruder, etc., have been well understood [9–13]. However, limited attention was paid to the morphology development of the previously mixed blend in subsequent part fabrication process, especially injection molding compared to the cases in preparation of previous blends [4, 14–16]. This process is, to a great degree, more crucial to plastic parts because that their final microscopic structure is formed at this stage.

*Author to whom all correspondence should be addressed.

Injection molding is one of the most important and widely used processing techniques by which blends are fabricated into various plastic parts. The morphological anisotropy characteristic of injection-molded blends is primarily the result of orientation of phases along the complex melt flow lines during mold filling, which include the 'fountain flow' pattern at the melt front [17–27]. In this case, a very thin region of materials at the mold surface experiences elongational flow at the front of the fountain flow pattern and creates an oriented surface. Most of the materials possess a melt morphology determined initially by shear and elongational flow fields experienced prior to entering the mold followed in the mold filling stage by shear flow behind the front of the fountain flow pattern. The shear rate profile through the thickness creates a gradient in the melt morphology. The amount of the retained melt morphology after cessation of flow depends not only on the cooling rate, but also on other factors like blend composition, phase viscosity ratio, incorporation of a compatibilizer, etc. which determine the amount of relaxation that occurs before solidification of the melt [27–35].

Karger-Kocsis and Csikai [4] explored the structure-property relationship as well as the failure phenomenon of injection molded polypropylene (PP) blends modified with ethylene/propylene/diene terpolymer and thermoplastic polyolefinic rubber. It was found that during injection molding, a skin-core morphology was formed in both the continuous PP matrix as well as in the modified PP blends containing rubber particles of various deformation. The characteristics of the latter were in agreement with those described by the Tadmor flow model. The skin layer consisted of a thin pure PP layer, whereas the subsurface layer contained more or less elongated rubbery particles due to the elogational flow at the wall. The deformation of the rubbery particles decreased, but their concentration increased with increasing distance from the skin layer towards the core. The deformed particles were oriented tangentionally to the flow front profile. Recently, Karger-Kocsis and Mouzakis [20] studied the effect of the injection-molding induced skin-core morphology on the behavior of rubber-toughened polypropylene (RTPP) systems by using the essential work of facture method. RTPP with high ethylene/propylene rubber (EPR) showed no skin-core structure after molding and the EWF approach worked well in this case. In contrast, RTPP with low EPR exhibited a pronounced skin-core morphology: EPR depletion and enrichment was observed in the skin and core region, respectively. This morphology caused necking instead of crack growth in deeply double edge-notched specimens under tensile loading along the molding filling direction. The necking process not only was accompanied by a large scatter but also yielded highly unrealistic specific essential work of fracture values. Fellahi *et al.* [15, 36] have performed the morphological study of injection molded HDPE/PA6 blends with and without a compatibilizer, in which the dispersed phase was highly oriented in the subskin and (spherical in the core, and interfacial modification results in a more stable morphology displaying a reduced phase size as well as a diminution of the thickness of the skin). In contrast to Karger-Kocsis' [4] acclamation that only pure matrix existing in the surface of the injection molded blend, Fellahi *et al.* found that, regardless of the apparent absence of dispersed phase as observed by SEM due to the very fine size of the dispersed phase in the skin relative to the core, the detailed compositional analysis by differential scanning calorimetry thermograms and X-ray photoelectron spectroscope revealed the presence of both matrix and dispersed phase on the surface of the injection molded blend at approximately the same composition as in the original blend. Son [16, 18] investigated the influence of phase viscosity ratio, injection molding condition and reactive compatibilization on the morphology of injection molded poly(phenylene oxide)/PA6 blends, where a distinct skin layer, subskin layer, and core region were found across the part thickness. For low viscosity ratios, small and large particles coexisted in the subskin layer, implying that both coalescence and breakup of the dispersed phase occurred in that layer. For high viscosity ratios, an intermediate zone, in which little deformation of the dispersed phase occurred, was found between the skin layer and the subskin layer. The injection flow rate primarily influenced the position of the subskin layer, and the injection temperature affected the aspect ratio of the dispersed phase. The reactive compatibilization reduced the flow-induced deformation, the coalescence and the breakup of particles and improved the dispersion of the minor phase.

Generally, injection molded blends with specific properties have quite different detailed skin-core morphology owing to the complicated relationship among the blend rheological behaviors and the complex shear, elongational flow as well as temperature fields. Great effort is needed to fully understand the injection-induced morphologies. There are few studies on the blend systems especially on the comparison of injection-molded blends with different nature properties as well as the relationship between morphology and mechanical properties.

The objective of this study and a subsequent one [37] is to investigate the injection-induced morphology of two immiscible blends, poly(ethylene terephthalate)(PET)/polyethylene(PE) and polycarbonate(PC)/PE, and its influences on the tensile behavior of the injection molded blend bars, with the emphasis on the difference of the two. PET/PE and PC/PE blends were chosen because PET/PE is a typical semicrystalline/semicrystalline polymer system with a viscosity ratio less than unity, and PC/PE a typical amorphous/semicrystalline polymer system with a viscosity ratio higher than unity.

2. Experimental

2.1. Materials

The resins used in this study were high density PE, PET and PC, where PET and PC were used as the dispersed phase and PE as the matrix. PE (5000S) was purchased from DaQing Petroleum Chemical Co., China. Its melt flow rate (MFR) is 0.9 g/10 min at 190°C, exerting a

TABLE I Characterization of PET, PC and PE resins

Characteristics	PET	PC	PE
Melt flow rate (MFR) (g/10 min)			0.90
Melting temperature by DSC (°C)	265		137
Glass transition temperature (°C)	75	147	
Torque for 5 min mixing at 280°C in a Haake rheometer (Nm)	0.37	37.5	9.5
Number average molecular weight ($M_n \times 10^4$)	2.1	2.8–3.2	52.81
Poisson's ratio	0.40	0.40	0.42
Young's modulus (MPa)	2900	2300	985
Yield strength (MPa)	78	60	20.5

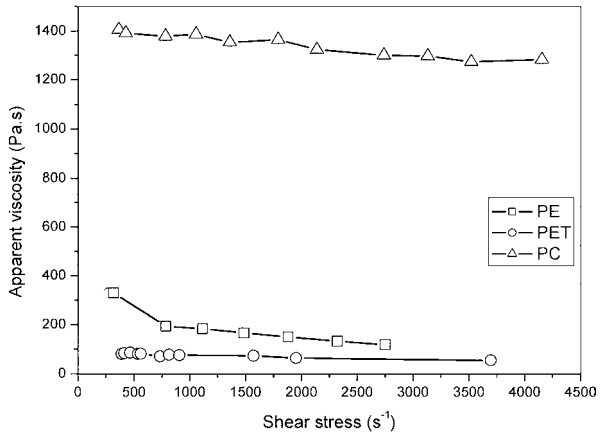

Figure 1 Apparent viscosity of PET, PC and PE resins as a function of shear rate at 280°C.

force of 21.6 N. PET pellets(textile grade)was supplied by UBE Co., Japan. PC (K1300) obtained from Teijin Chemical Co. Ltd., Japan is derived from bisphenol A. Their properties, including the number molecular weight, are summarized in Table I, and their rheological behavior is shown in Fig. 1, which was obtained using a Haake rheometer at 280°C with a capillary die of 0.127 mm diameter and a length to diameter (L/D) ratio of 40.

2.2. Preparation and injection molding of PET/PE and PC/PE blends

PET and PC were dried for 12 h before processing under vacuum at 100°C to avoid the hydrolytic degradation of PET and PC. PET and PC were dry-mixed with PE respectively in a fixed weight ratio of 15/85 throughout this study. The mixture was then blended in a twin-screw extruder with a temperature profile: 190, 230, 250, 265, 275 and 280°C from hopper to die. The screw speed was maintained at 120 rpm. The extrudate in the form of thread extruded through a rod die was pelletized and dried before injection molding. The dog-bone specimens as shown in Fig. 2 were molded using a PS40E5ASE model injection molding machine made in Nissin, Japan. The mold used had two-cavities and a single gate in each cavity which assured no weldline in the specimen. Injection molding parameters were listed in Table II, which generally included two groups, low and high injection speed. The temperature profile used was 240, 265, 275 and 270°C from hopper to nozzle.

TABLE II The injection processing parameters used

Parameters	Group 1 low injection speed	Group 2 high injection speed
Injection speed (m/s)	10.0	23.9
Injection flow rate (m^3/s)	3.23×10^{-6}	7.73×10^{-6}
Total cycle time (s)	55.0	52.8
Injection time (s)	5.5	2.3
Holding pressure time (s)	12	12
Cooling time (s)	40	40
Injection pressure (MPa)	80	80
Hold pressure (MPa)	75	75
Back pressure (MPa)	40	40
Screw speed (rpm)	100	100
Mold temperature (°C)	40	40

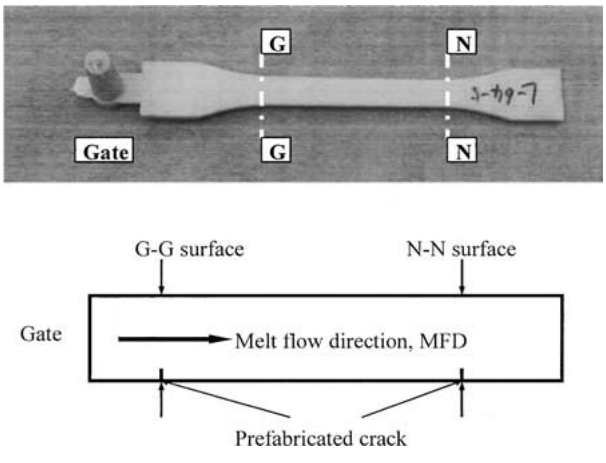

Figure 2 Injection molded dog-bone specimen and the positions for SEM observation.

2.3. Morphological observation

The phase morphology was characterized with a JEOL JSM-5900LV scanning electron microscope (SEM). The specimens were frozen in liquid nitrogen for one hour then impact broken to make surfaces for observation. The positions of the fracture surfaces on the specimens were fixed by making a prefabricated flat crack in one side perpendicular to the melt flow direction with a fresh razor. Two fracture surfaces for each blend were observed, one close to the gate (refered to as surface G-G) and the other close to the non-gate end of the specimen (see Fig. 2). Prior to examination, the surfaces were covered with a layer of gold to make them conductive.

3. Results and discussion

3.1. Initial morphology of PET/PE and PC/PE blends

Before SEM micrographic study, the extruded PET/PE and PC/PE blends were mixed again in a static internal mixer at the processing temperature (170°C) of PE. The SEM micrographs of the mixed blends were shown in Fig. 3. It is clear that the PET and PC particles exhibited spherical and ellipsoidal forms, and the diameter of the particles showed a range of distribution. Recalling the fact that the post mixing temperature in the mixer is far below the melting temperature of PET and the flow

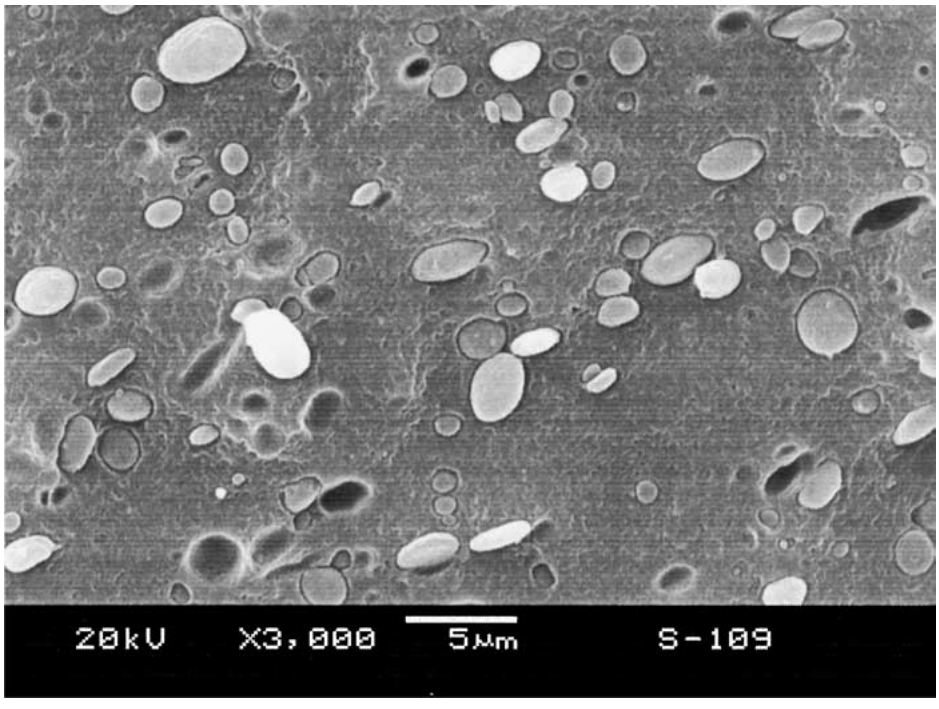

(a)

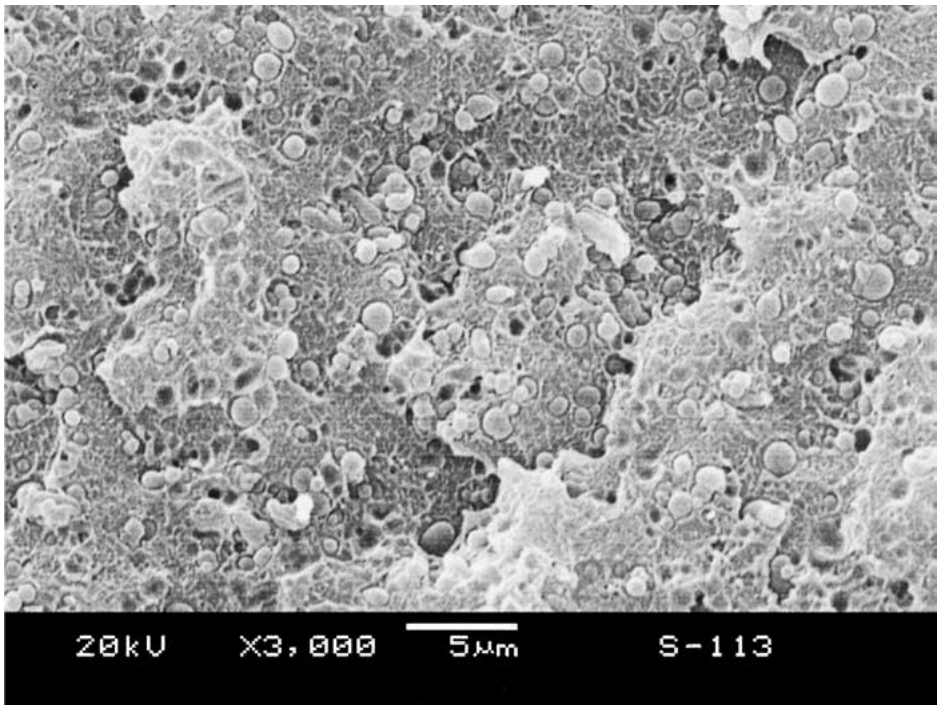

(b)

Figure 3 Initial morphology of PET/PE and PC/PE blends: (a) PET/PE blend and (b) PC/PE blend.

temperature of PC, it is evident that the dispersed particles shown were the ones generated during twin-screw extrusion [38]. The interfaces of the blends were very smooth and there was no evidence of any adhesion, indicating that these two blends were extremely incompatible. The dispersed PET and PC particles showed tight contact with PE matrix leaving no distinct voids between the particles and matrix. This resulted from the fact that there was no phase transition for PET and PC from 170°C to room temperature, while high contracting of PE matrix onto PET and PC particles occurred due to the high crystallization shrinkage of PE during this temperature range.

The average, minimum and maximum diameters of PET and PC particles are summarized in Table III. It

TABLE III The average, minimum and maximum PET and PC particle diameters obtained from the SEM micrographs

Blends	Min. Max. diameter (μm)	Average diameter (μm)
PET/PE	0.4–3.5	1.2
PC/PE	0.2–1.5	0.7

was found that the minimum, maximum and average diameters of PET particles were larger than those of PC particles respectively. This may be caused by the different polarity of the macromolecular chains of PET and PC as claimed by Min and White [39]. They observed that the higher the molecular polarity of polymers, the larger the domain size of the dispersed phase in the blends.

3.2. Overall survey of the morphology for injection molded PET/PE and PC/PE blends

SEM micrographs of injection molded PET/PE and PC/PE blends over the cross section from the surface to the center are presented in Fig. 4 through Fig. 7. The diameter change of the dispersed phase across the specimen thickness is shown in Fig. 8. The minimum,

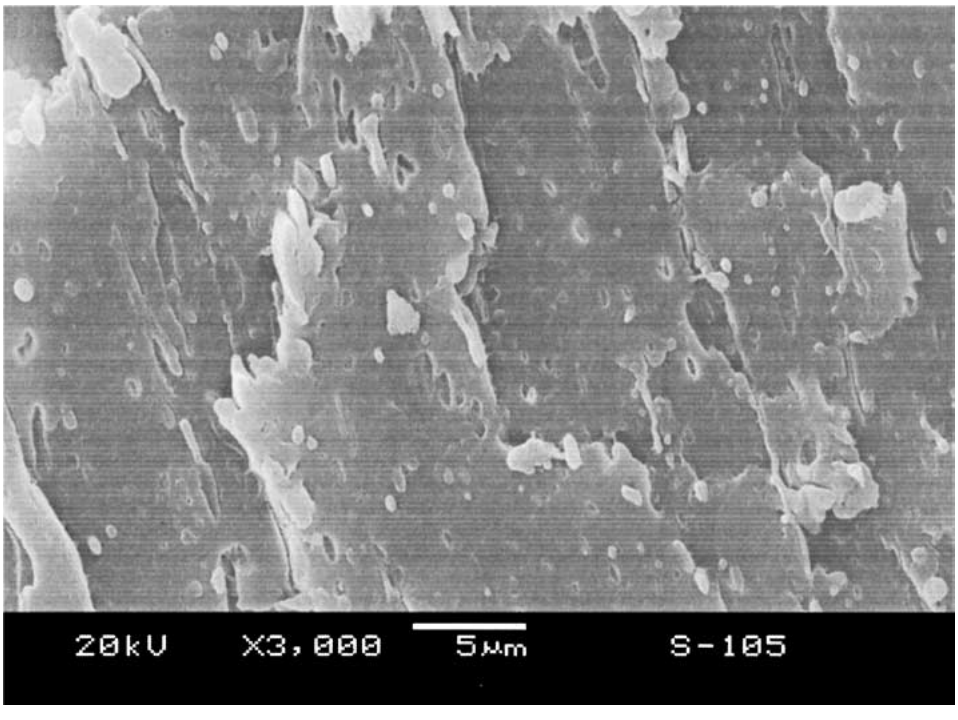

(a)

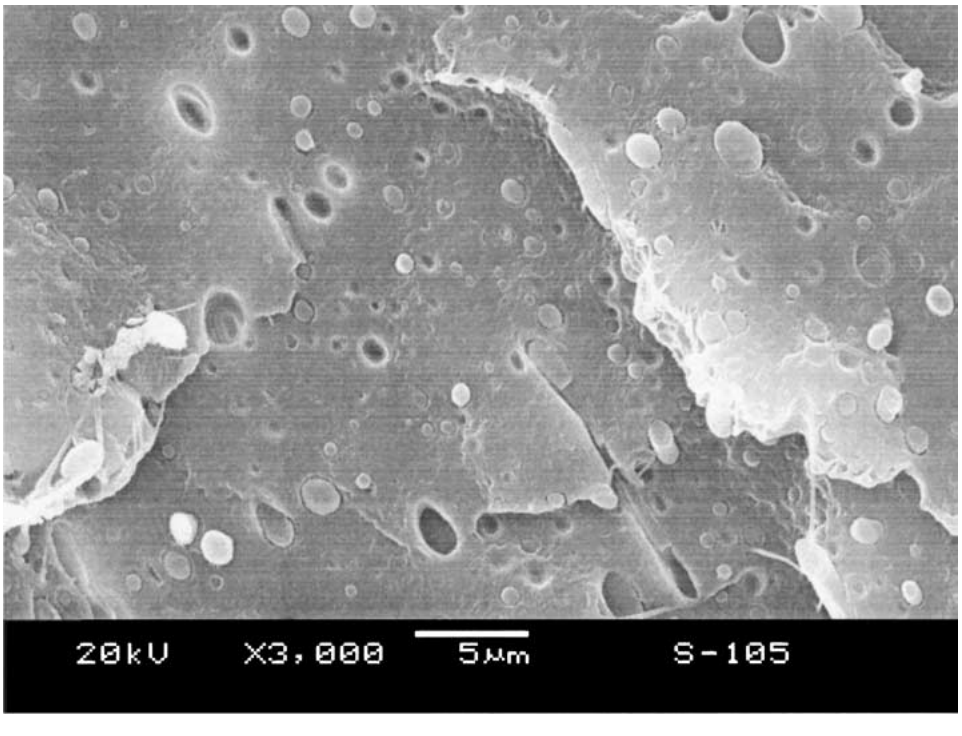

(a′)

Figure 4 SEM micrographs about G-G (close to the gate end) and N-N (close to the non-gate end) surfaces of PET/PE blend at different positions molded with low injection speed: (a) and (a′): subskin; (b) and (b′): intermediate zone; (c) and (c′): core (a), (b) and (c): G-G surface; (a′), (b′) and (c′): N-N surface. (*Continued*)

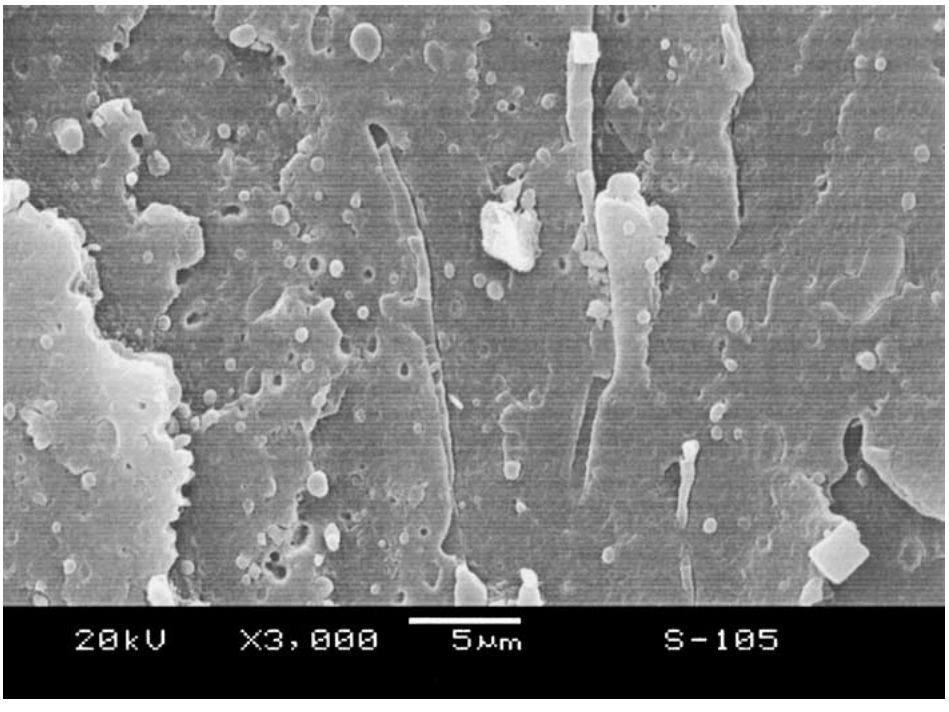

(b)

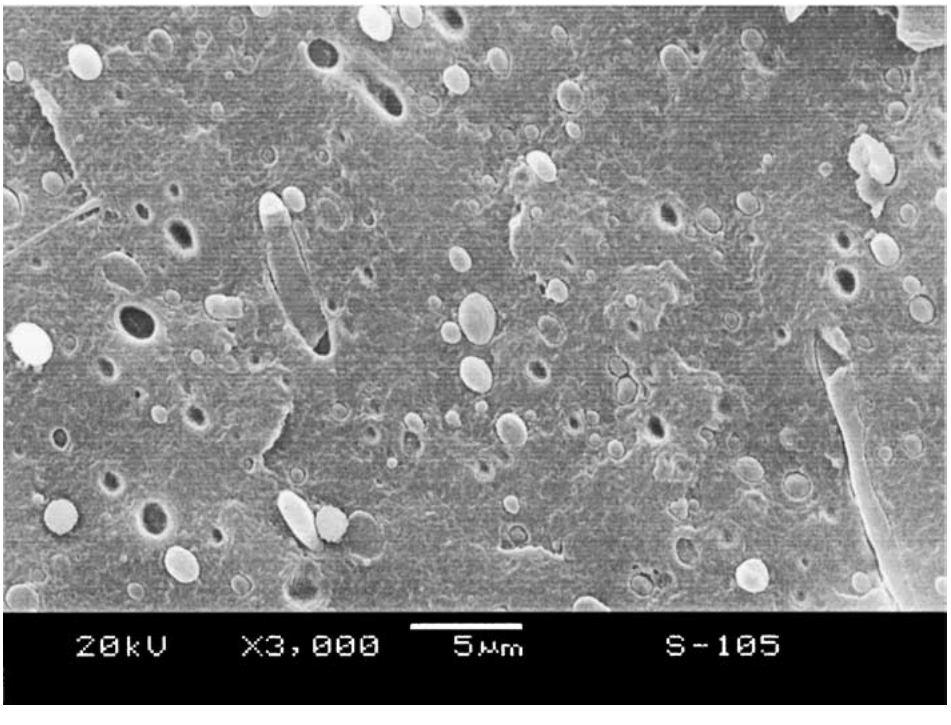

(b′)

Figure 4 (*Continued*).

maximum and average diameter of dispersed phase domains for injection molded PET/PE and PC/PE blends obtained from SEM observation are listed in Table IV. The morphology inside the molded specimens for all cases was apparently heterogeneous and anisotropic, generally assuming a typical skin-core distribution, in agreement with some earlier observations in some injection molded immiscible polymer blends [4, 14, 15]. The subskin layer consisted of more or less elongated particles and they showed different degrees of deformation. At low injection speed, the PET/PE blend showed mainly ellipsoidal particles, while PC/PE blend showed well-defined fibers. The deformation degree of the dispersed particles decreased from the skin layer towards the core, as shown in Fig. 8. And also the diameter of the dispersed PET and PC particles increased from the skin layer towards the center. In the core layer, the dispersed phase mainly assumed the form of sphere. Moreover, both blends exhibited an intermediate layer where elongated particle/spherical particle transition took place. For both PET/PE and PC/PE blends, owing to the poor adhesion between the matrix and the

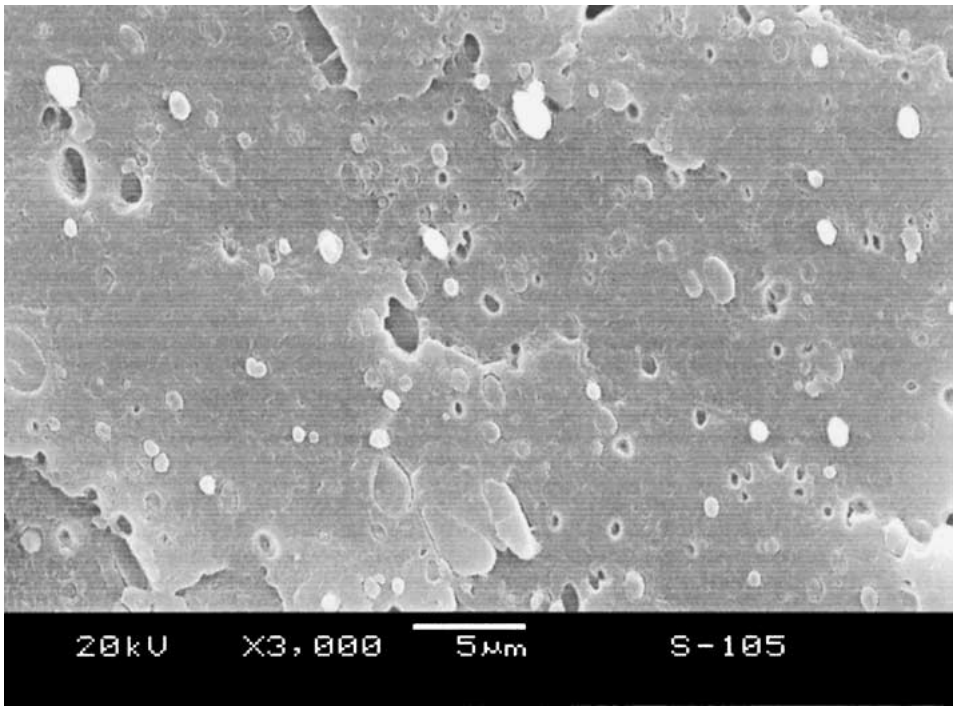

(c)

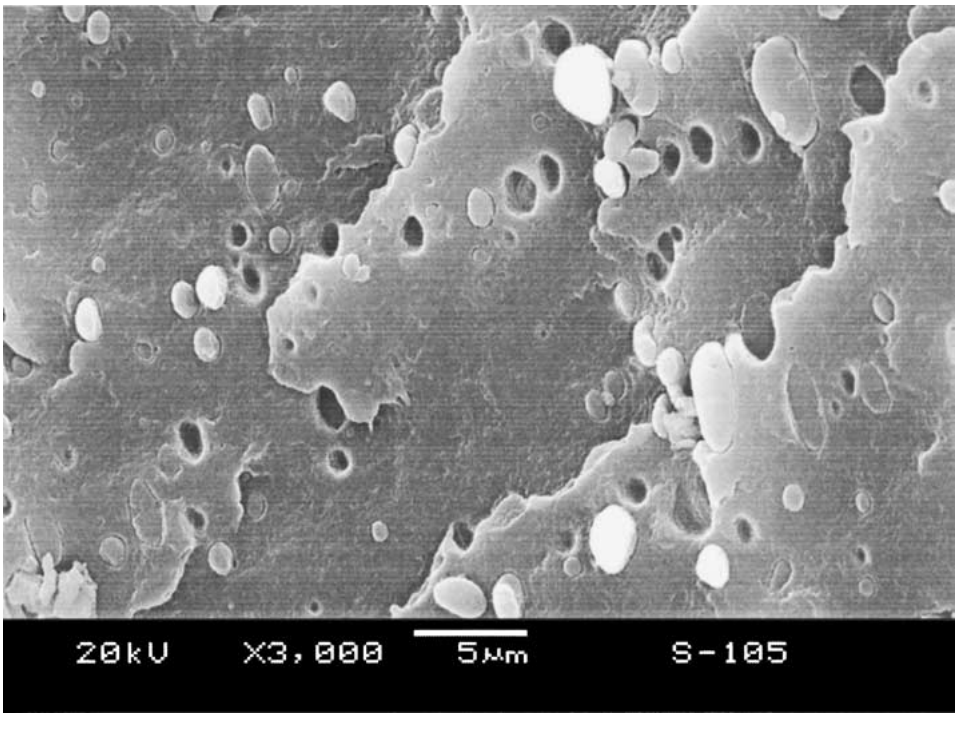

(c′)

Figure 4 (*Continued*).

dispersed phase, stretched dispersion particles/fibers were pulled out from PE matrix during the fracture, leaving naked ellipsiodial particles/fibers and holes on the observation surface.

3.3. Morphology comparison between gate end and non-gate end

The single-gate cavity was used in this study, so the mold was filled successively from the gate to the non-gate end. If there is a difference in morphology between the gate end and the non-gate end, the transition should be continuous from the gate end to the non-gate end. Therefore the detailed morphology evolution along the specimen could be conjectured by studying the morphology at the gate and non-gate end. The following results were obtained by comparing the micrographs in Figs 4–8:

1. For the PET/PE blend, the PET particles in the subskin layer at gate and non-gate ends assumed

spherical or ellipsoidal forms at low injection speed, and fibrillar form at high injection speed. In contrast, for the PC/PE blend, at both injection speeds, the dispersed PC phase in the subskin layer was basically fibrous.

2. For the same layer (subskin, intermediate or core layers) the diameter of the dispersed phase at the non-gate end was generally larger than that at the gate end indicating that larger deformation took place at the gate end than at the non-gate end of the specimens.

3. For the same layer, the size distribution (the difference between the minimum and the maximum diameters) of the dispersed phase at the non-gate end was generally wider than that at the gate end. This indicated

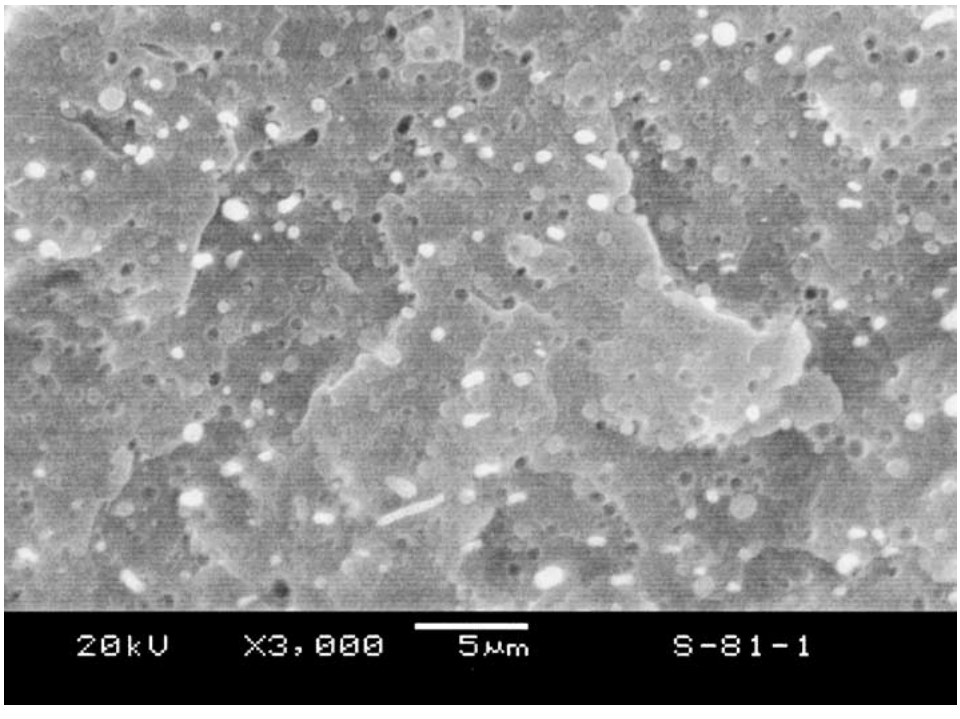

(a)

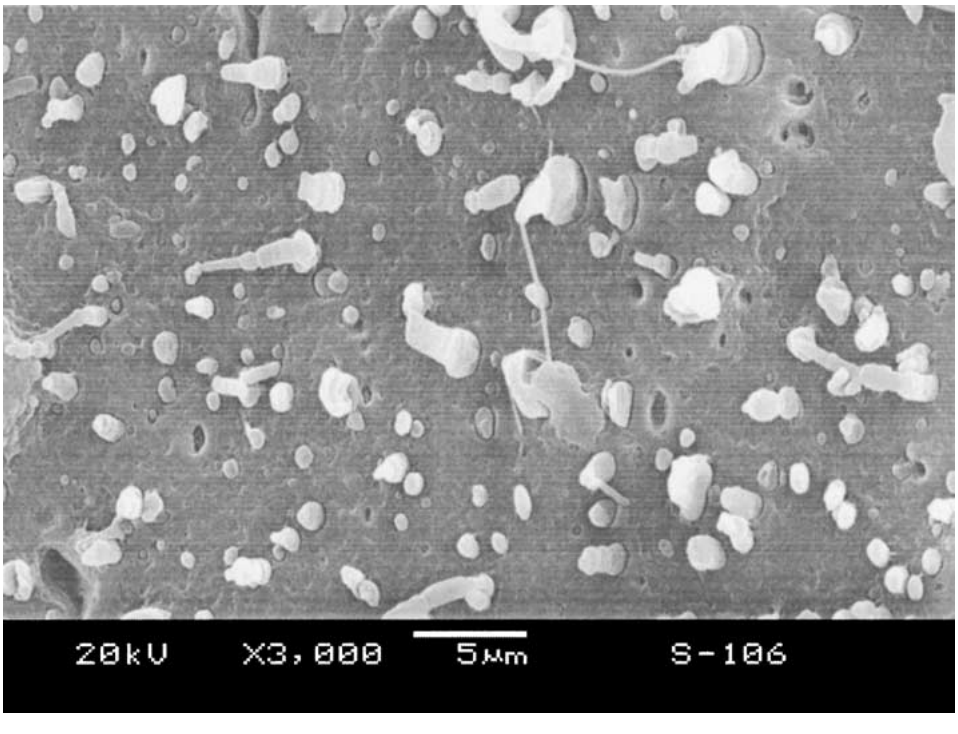

(a′)

Figure 5 SEM micrographs about G-G (close to the gate end) and N-N (close to the non-gate end) surfaces of PET/PE blend at different positions molded with high injection speed: (a) and (a′): subskin; (b) and (b′): intermediate zone; (c) and (c′): core. (a), (b) and (c): G-G surface; (a′), (b′) and (c′): N-N surface. (*Continued*)

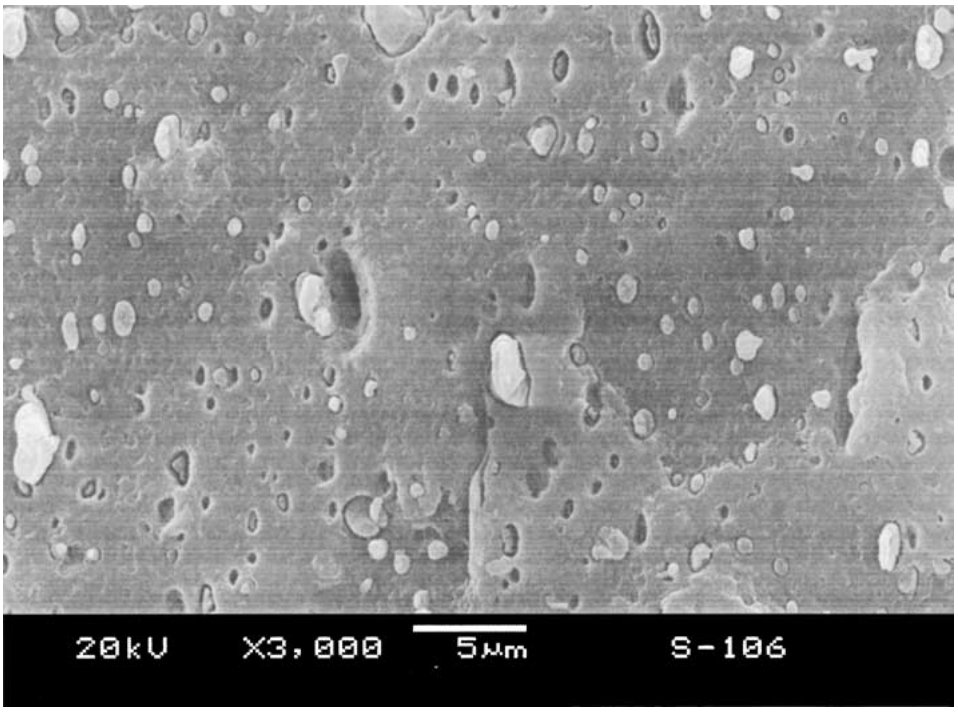

(b)

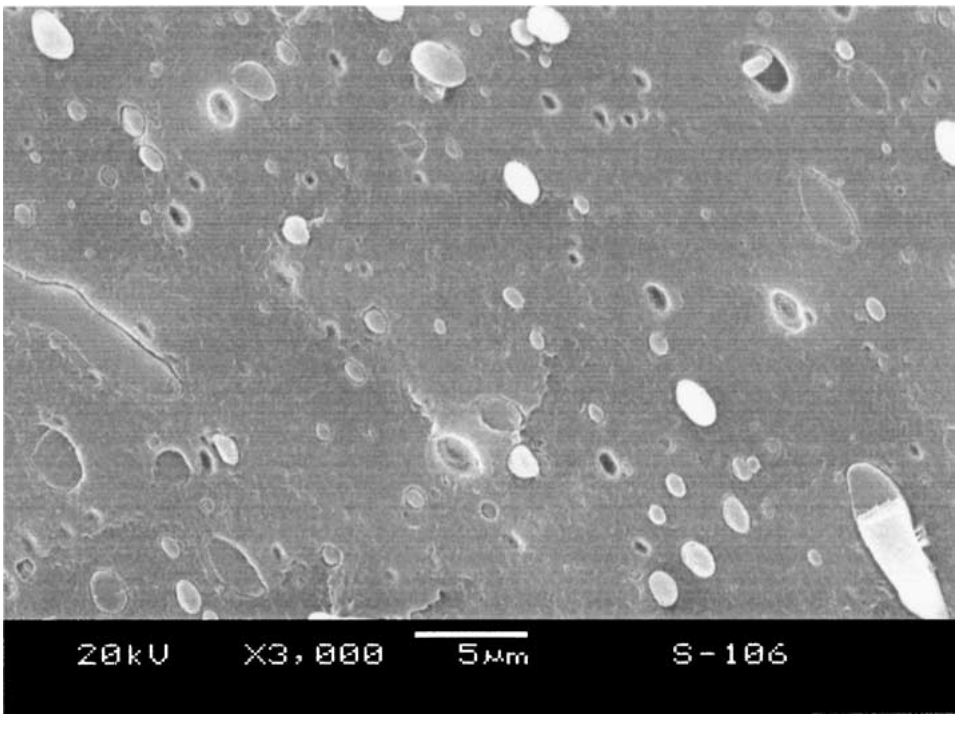

(b′)

Figure 5 (*Continued*).

that more irregular deformation happened at the non-gate end of the molded bar.

4. The thickness (the distance from the surface layer to the intermediate layer) of the subskin layer reduced along the bar from the gate to the non-gate end, as shown in Fig. 8. Besides, the PET/PE blend had a thicker subskin layer than PC/PE blend. For example, at low injection speed, the subskin layer thickness of the PET/PE blend at the gate end and non-gate end was about 0.7 and 0.4 mm respectively, whereas for the PC/PE blend, it was 1.1 and 0.8 mm.

3.4. Morphology comparison between the blends injection molded at low- and high-injection speeds

In practical injection molding, an appropriate injection speed is needed to fill the mold properly. If the injection

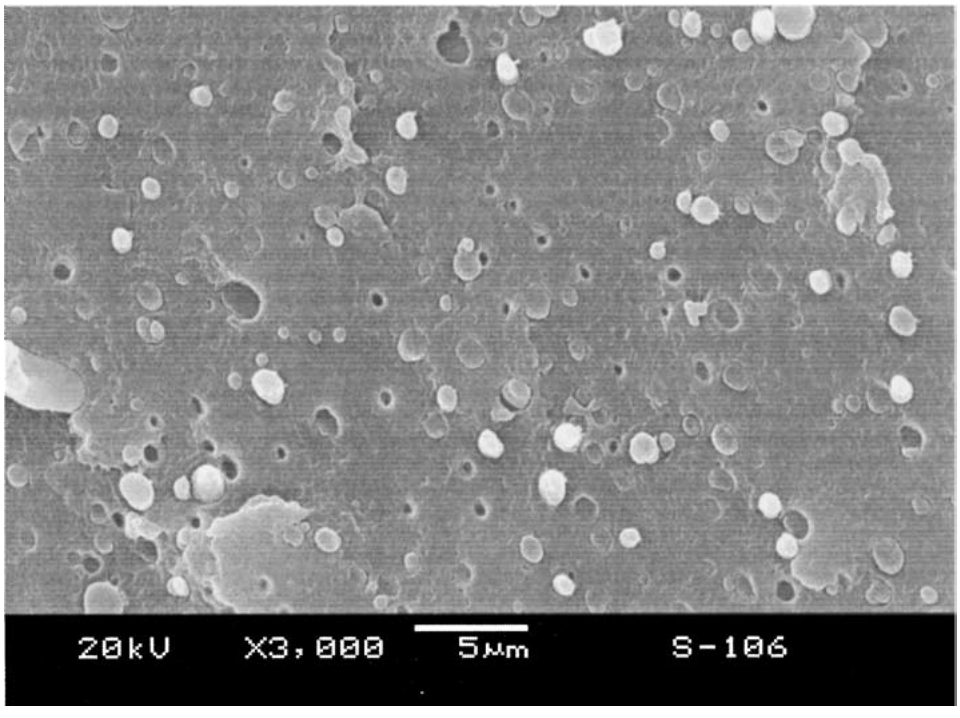

(c)

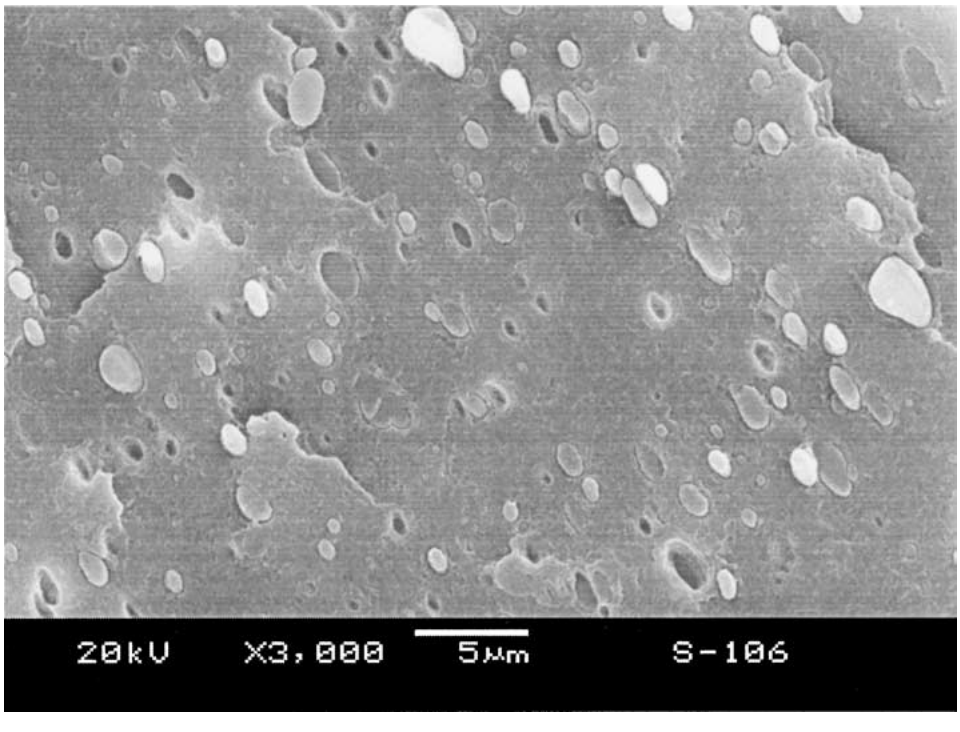

(c′)

Figure 5 (*Continued*).

speed is too low, a short shot is obtained. The effect of injection speed on the morphology could be observed from Figs 4–8.

1. High injection speed facilitated the fibrillation of the dispersed phase in the subskin layer. Especially for the PET/PE blend, the PET phase was mainly ellipsoidal in the subkin layer at low injection flow rate, while it was fibrous at high injection speed.

2. Injection speed had a somewhat different effect on the diameter and its distribution of the dispersed phase in PET/PE and PC/PE blends. At high injection speed, the average diameter of the dispersed PET phase was smaller and the distribution was wider than PC phase.

3. It was clear from Fig. 8 that, for both blends, the distance from the intermediate layer to the surface was larger for the high injection speed bars, indicating that the subskin layer or fibrous layer was thicker.

3.5. Origin of the morphology development for PET/PE and PC/PE blends

The results obtained above indicated that the morphology of the injection molded PET/PE and PC/PE blends were very complicated. The shape and size of the PET and PC phases depended not only on the material properties of the PET/PE and PC/PE blends, but also on the injection molding parameters like injection speed as well as the positions throughout the entire molded bar. The morphology of the entire section along the specimen along the melt flow direction was schematically illustrated in Fig. 9. The thickness of the sub-skin layer containing fibrous structure gradually decreased along the molded bar from the gate to the non-gate end. In the core region, the dispersed phase was mainly present as spherical particles whose diameter increased along the melt flow pathway. Between these two layers, there was an intermediate layer where the dispersed

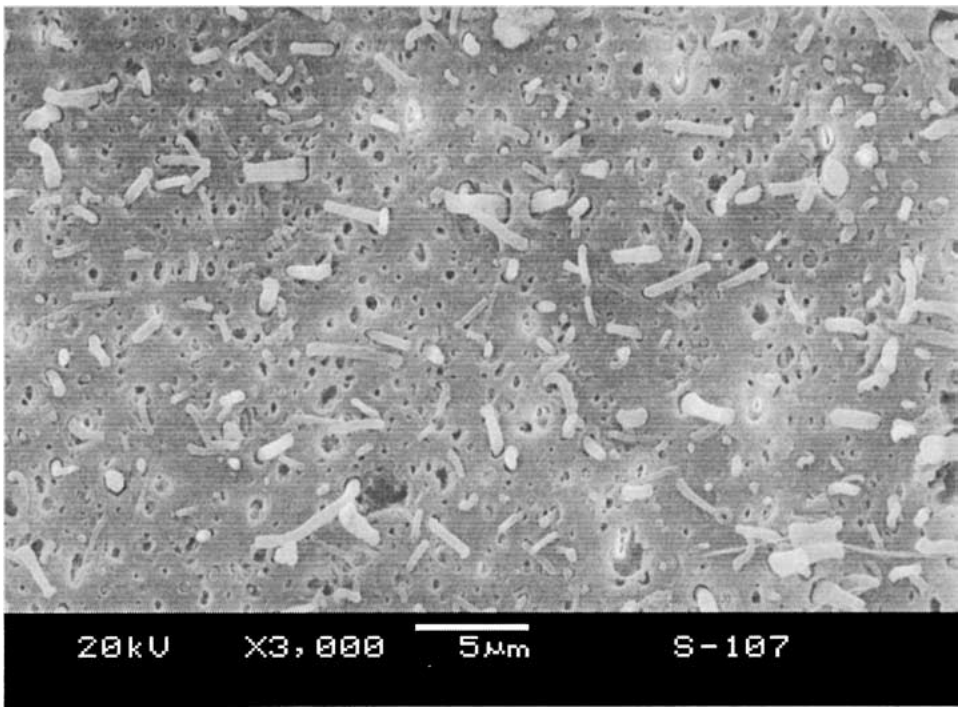

(a)

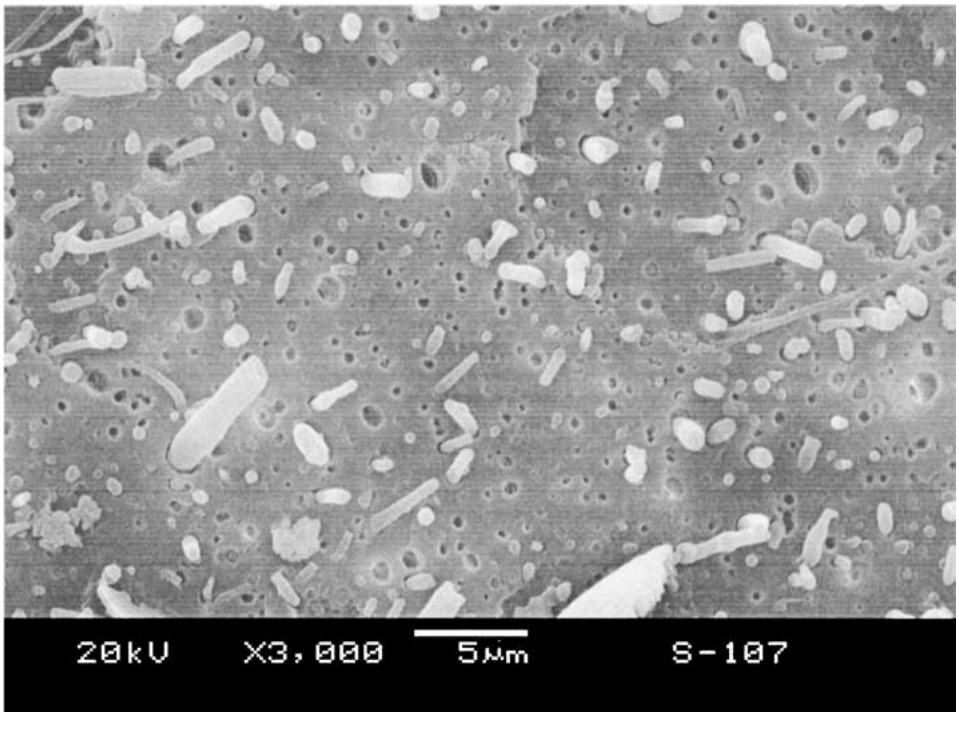

(a′)

Figure 6 SEM micrographs about G-G (close to the gate end) and N-N (close to the non-gate end) surfaces of PC/PE blend at different positions molded with low injection speed. (a) and (a′): subskin; (b) and (b′): intermediate zone; (c) and (c′): core. (a), (b) and (c): G-G surface; (a′), (b′) and (c′): N-N surface. (*Continued*)

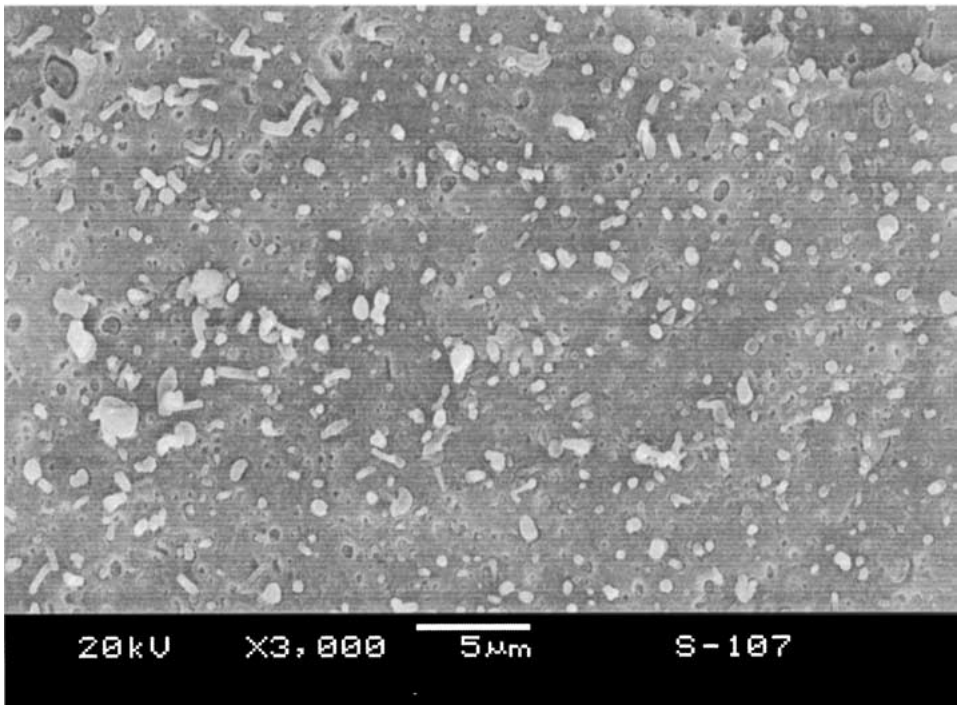

(b)

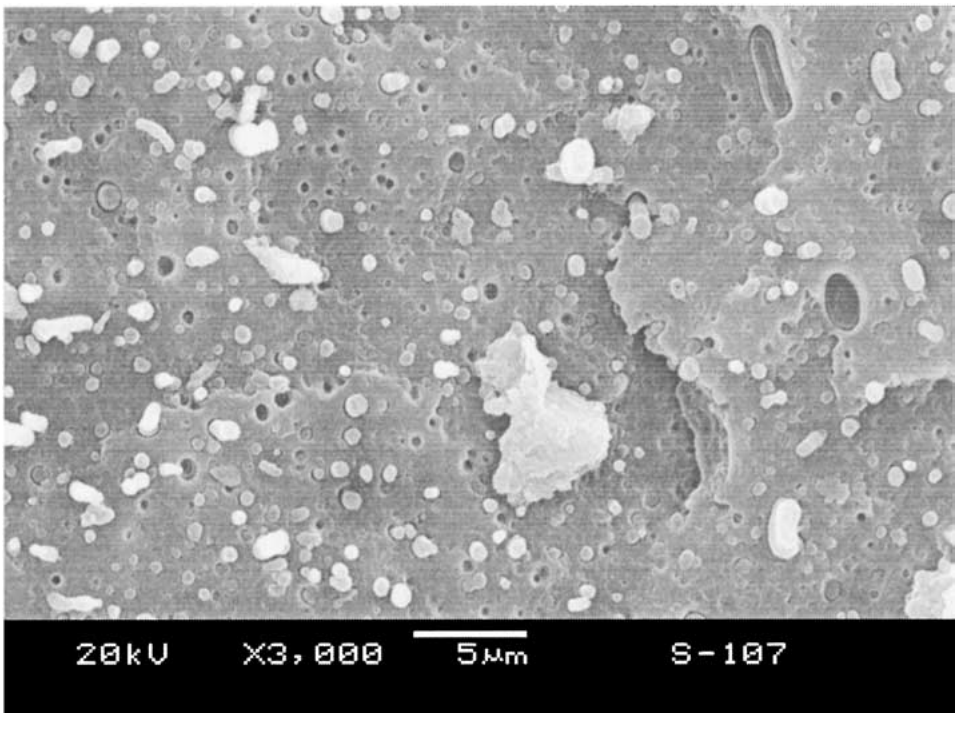

(b′)

Figure 6 (*Continued*).

particles mainly assumed the form of fibers, ellipsoids or spheres. The trend of the size change from gate to non-gate end was the same as other two layers. It needs to be pointed out that the diagram in Fig. 9 was not appropriate to the PET/PE blend molded at low injection speed since there no clearly fibrous structures were observed.

Deformation of a dispersed phase in an incompatible polymer blend has long been studied to understand rheologically and morphologically the nature of deformation of a blend during processing [40–42]. It is well known that the morphology resulting from blending and processing depends mainly upon the rheological and interfacial properties, the viscosity ratio, the blend composition, the mixing parameters and the mixing mode. For Newtonian systems [43, 44], the dispersed phase deformation process is controlled by the viscosity ratio $p = \eta_d/\eta_m$ and the capillarity number $Ca = \eta_m\gamma/(\sigma/R)$, where η_d is the viscosity of the dispersed phase, η_m the matrix viscosity, γ the shear rate,

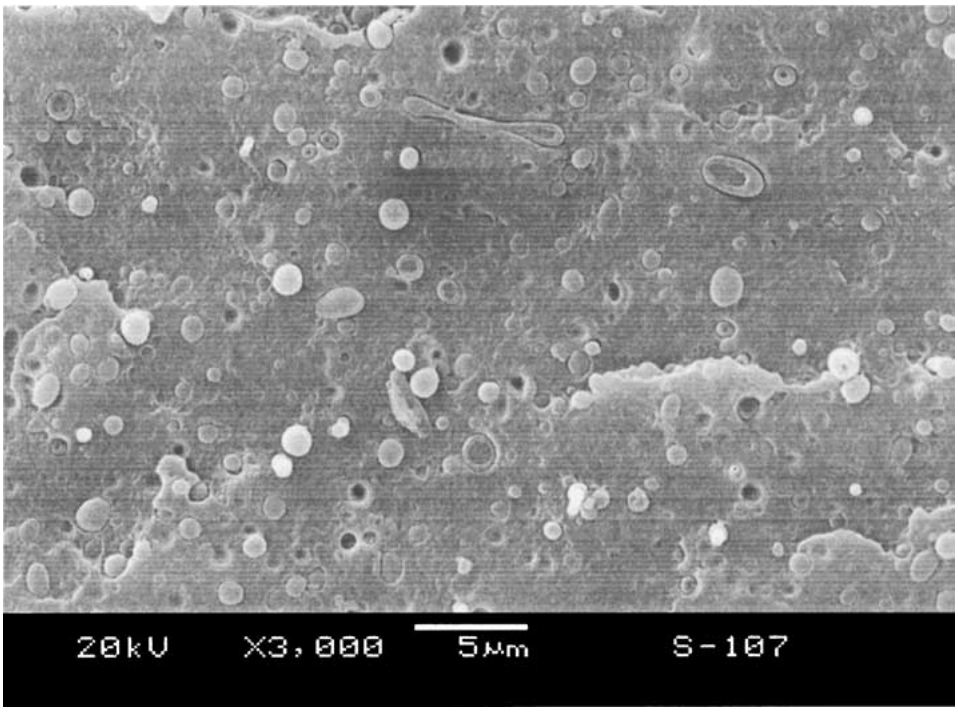

(c)

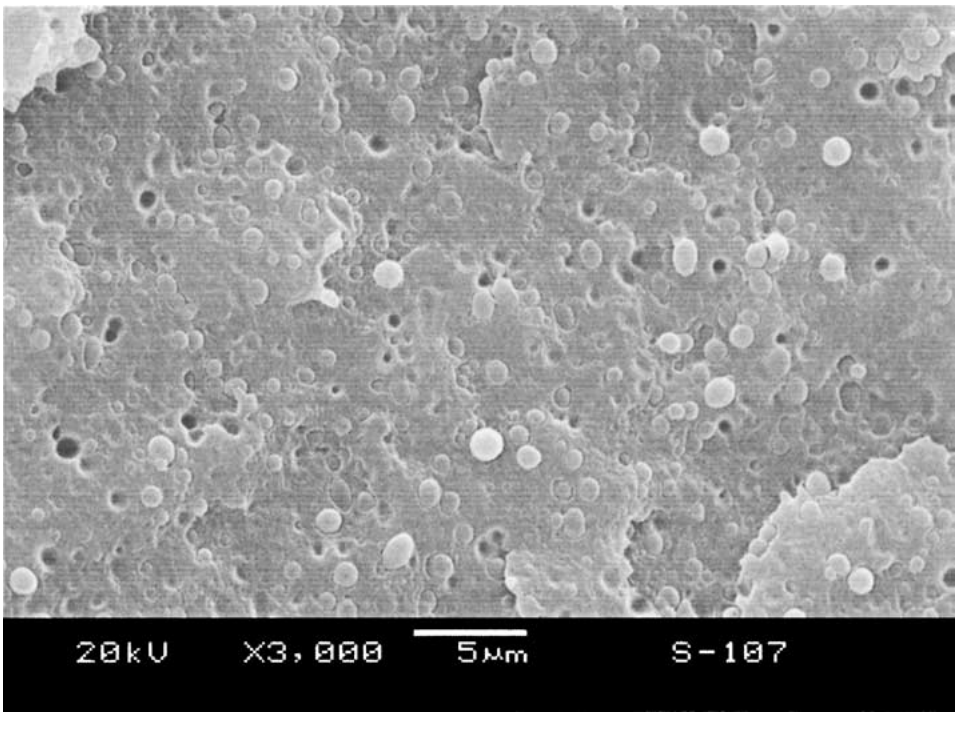

(c′)

Figure 6 (*Continued*).

σ the interfacial tension, and R the dispersed particle radius. The capillarity number Ca can be understood as the ratio between the hydrodynamic stress $\eta_m\gamma$ acting to deform the particle, and the interfacial stress σ/R leading to minimize the surface energy and to keep the particle in its equilibrium spherical shape. Beyond a critical value Ca_{crit} of the capillarity number, the particle will be elongated and may break up into smaller droplets. The value Ca_{crit} has been revealed to depend strongly on the viscosity ratio p as well as on the type of flow, simple shear or elongational flow. Many studies have shown that an elongational flow field and a small viscosity ratio (usually less than or close to unity) facilitate the deformation (especially fibrillation) of the dispersed phase in the polymer blend [10, 45–47]. PC is much more viscous than PET in the molten state. Therefore, the viscosity ratio differs greatly between PET/PE and PC/PE blends. The viscosity ratio of PET/PE blends is much lower than unity, while that of PC/PE is much higher than unity (see Fig. 1). Additionally, PC has

higher interfacial stress than PET. As a result, compared to PC, the dispersed PET phase has higher deformation capability under the same external conditions. But it tends to break up into smaller droplets and coalesce into larger domains if cooling to the final solid state is not rapid enough to maintain the deformation. Generally the diameter of PET particles is larger than that of PC particles regardless of the elongation of the dispersed phase. It seems that the coalescence has a dominant effect.

Before mold filling, the preformed dispersed PC and PET droplets must have already experienced some degree of stretching in the high shear and elongational flow fields during the previous blending process. The morphology evolution to the final solid-state structure after injection molding was determined by the flow

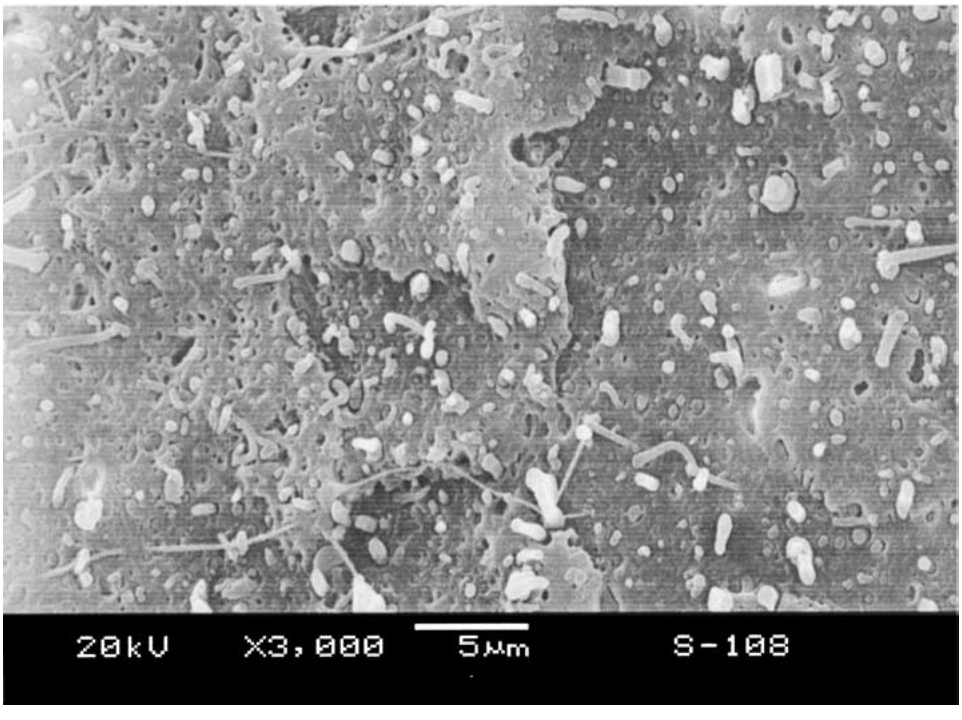

(a)

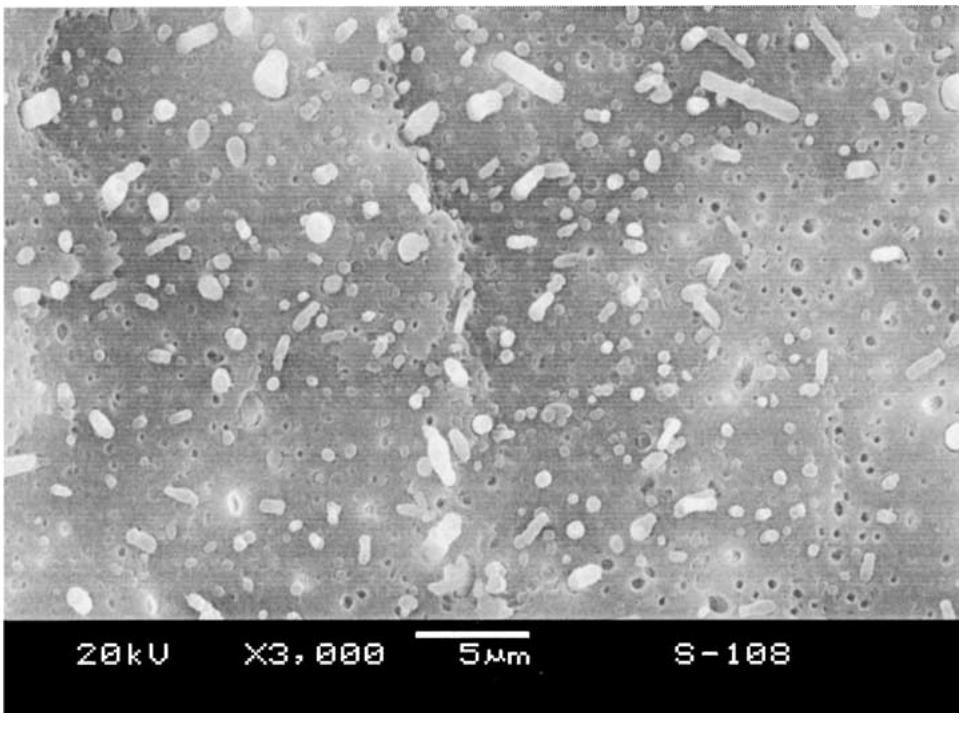

(a′)

Figure 7 SEM micrographs about G-G (close to the gate end) and N-N (close to the non-gate end) surfaces of PC/PE blend at different positions molded with high injection speed. (a) and (a′): subskin; (b) and (b′): intermediate zone; (c) and (c′): core. (a), (b) and (c): G-G surface; (a′), (b′) and (c′): N-N surface. (*Continued*)

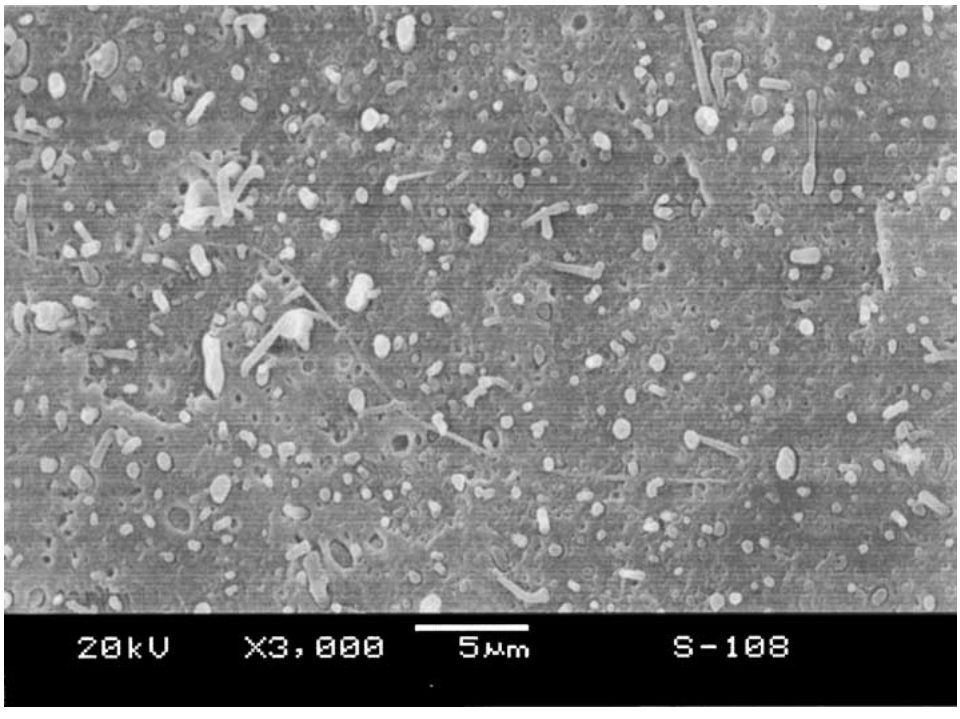

(b)

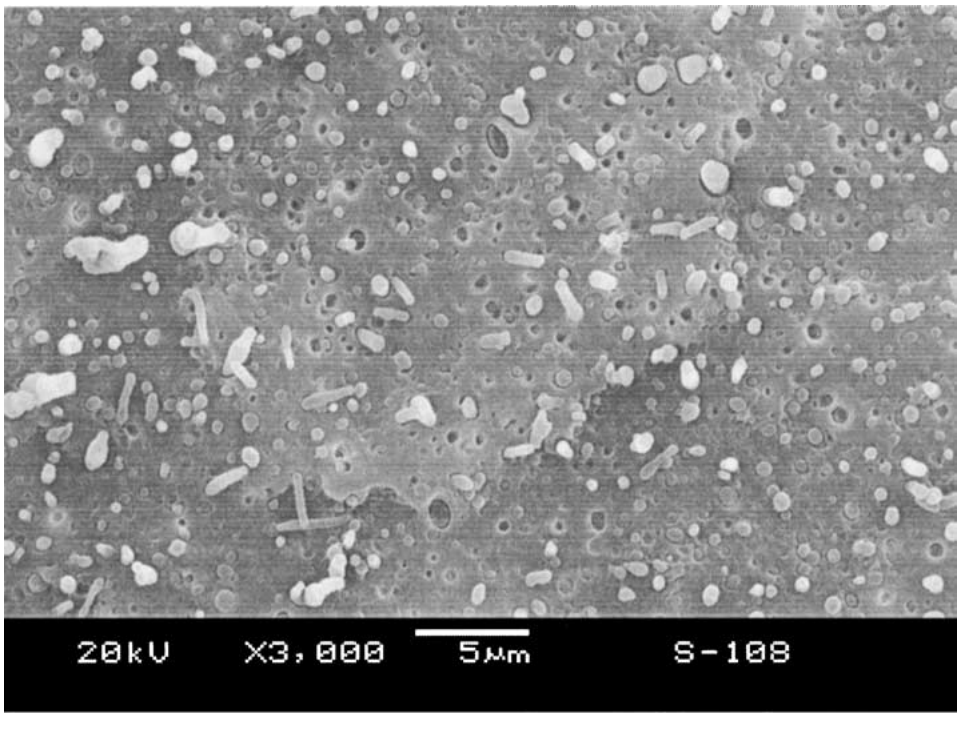

(b′)

Figure 7 (*Continued*).

fields experienced by the melt during mold filling, and the cooling rate during and after mold filling. The high shear and elongational fields during mold filling cause the deformation and also the break up and coalescence of the dispersed particles. The final shape and size of the injection-molded bar is the product of the balance between deformation, breakup and coalescence. In the case of non-isothermal flow, the velocity distribution across the thickness has an inflection point where the shear rate reaches the maximum [27], while the shear rate is zero at the mold surface and the center. The shear rate profile in two positions of the cross section from gate to non-gate end is schematically illustrated in Fig. 10. Compared to other shear rate profiles proposed in the literature [26], it presents a solidified layer with increasing thickness along melt flow direction. The solidified layer was formed continuously until cessation of mold filling. The solidified layer shown in Fig. 9 contained elongated dispersed phase. That the solid layer close to the gate end was thicker is understandable because of the following facts:

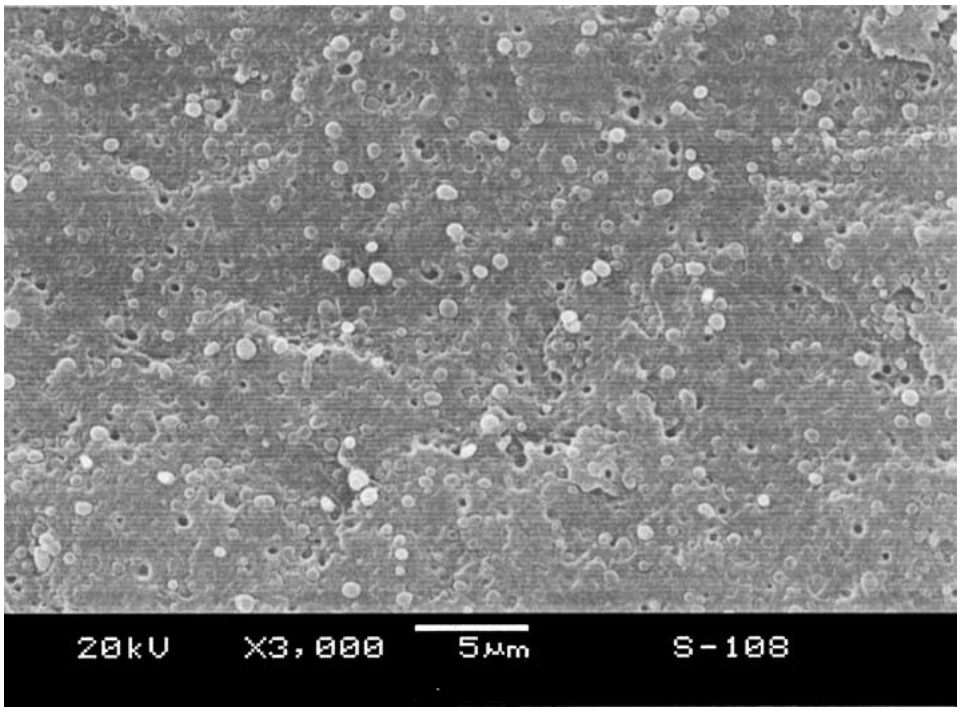

(c)

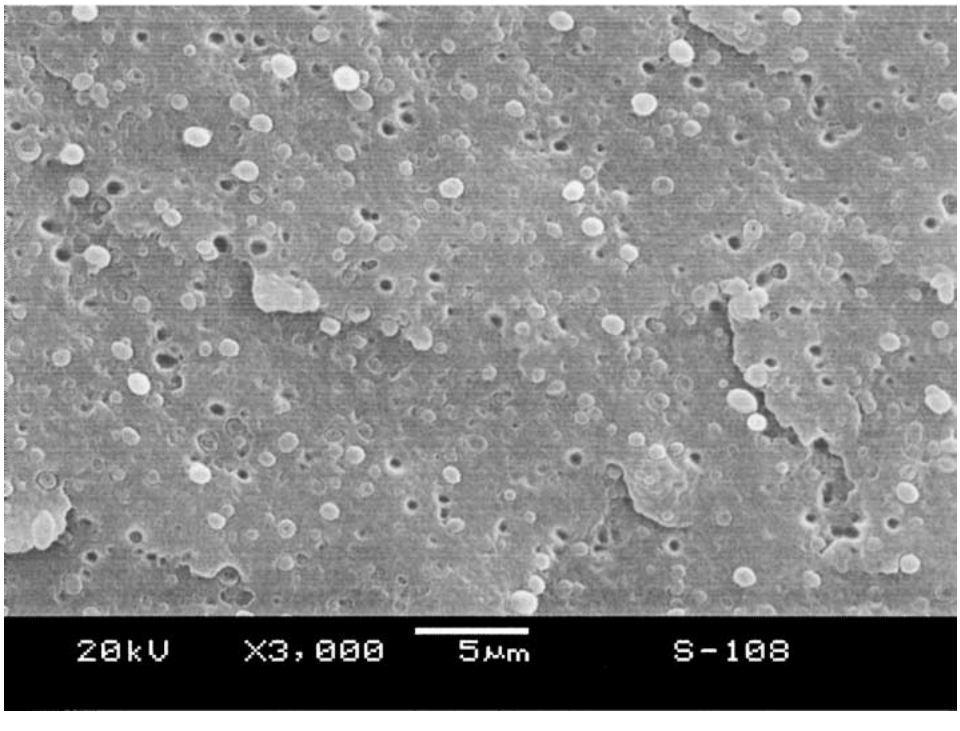

(c′)

Figure 7 (*Continued*).

1. Even though the same thickness forms as the melt flow front touches the cold mold surface all along the mold, the material near the initial solid layer can continue to cool to solid until the cessation of mold filling.

2. The solidified layer near the gate end experienced longer thickening time than that at the non-gate end.

3. As soon as the solidified layer is formed, the shear rate in the previously solidified layer surface decreases to zero. Though the maximum shear rate appears near the solidified layer surface, there exists a thin melt layer where the shear rate is relatively low since the shear rate changes continuously from zero at the surface of the solidified layer to the maximum at a point quite close to the solidified layer. Based on the same reason, the subskin layer, mainly comprised of elongated dispersed phase, turns thinner along the melt flow direction, while the core layer containing mainly spherical domains gets thicker and thicker from gate to non-gate end.

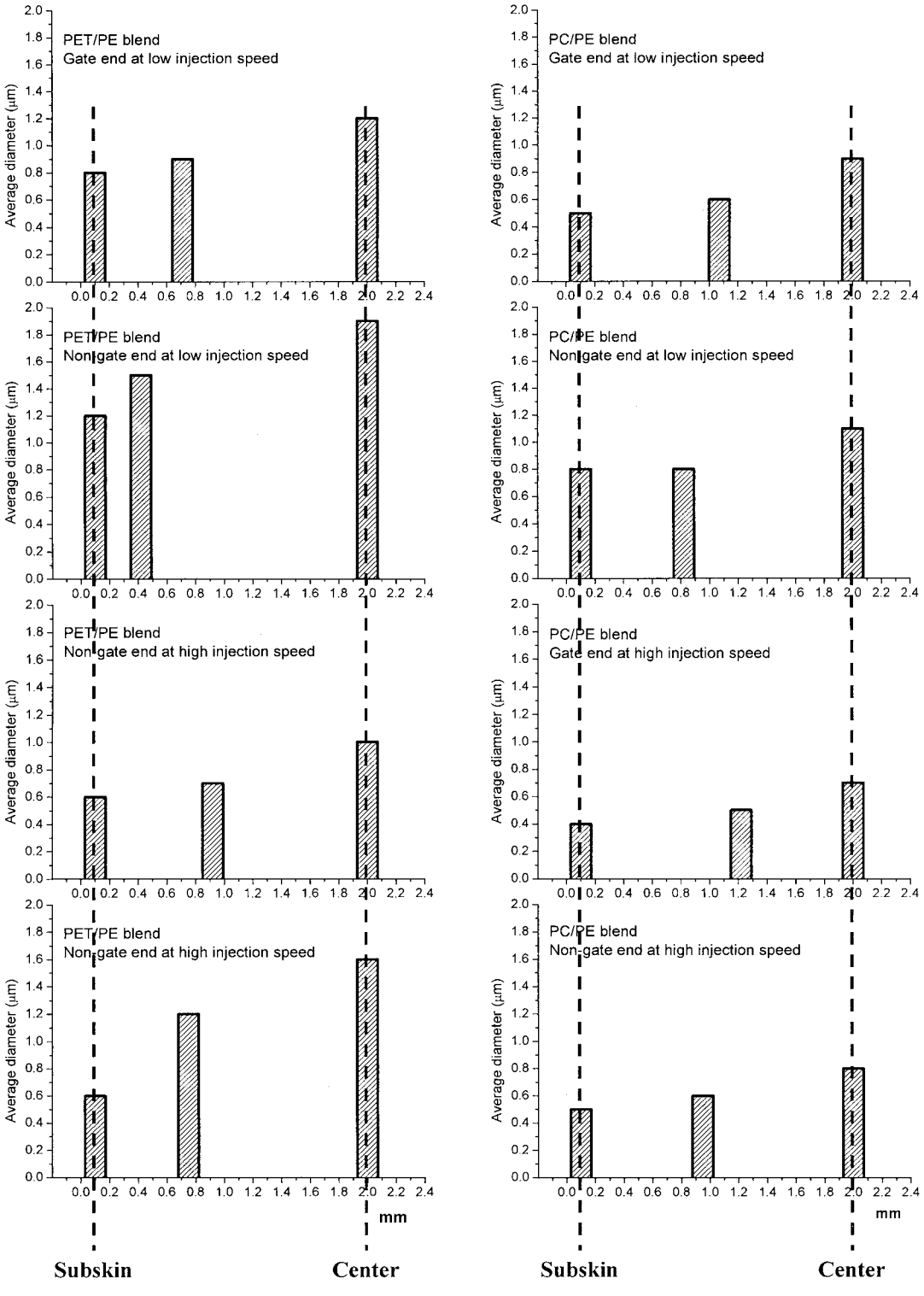

Figure 8 The diameter change of the dispersed phase across the specimen thickness. Note: X coordinate value of the middle column inside the figures represents the distance of the intermediate layer to the surface.

The higher the melt flow rate is, the shorter the time is needed for mold filling, and the stronger the shear and elongational fields are. Hence, high injection speed promotes the deformation and the breakup of particles. As mentioned above, the final morphology is the product of the balance between deformation and breakup. From Figs 3–8, it was found that the deformation played a predominant role in the formation of the subskin layer since with the increase of the injection speed, the diameter of the elongated particles decreased significantly. The increase of injection speed shifted the position of the subskin layer toward the bar surface (i.e., the solidified layer became thinner), increased the aspect ratio of the dispersed particles, and reduced the diameter of the dispersed particles in the subskin layer. Moreover, for high speed injection molding, after mold filling, the melt exhibited relatively higher temperature than the case of low speed injection because the melt was exposed less time to a cold mold and more heat was generated by the viscous friction during mold filling.

TABLE IV Minimum, maximum and average diameter of dispersed phase domains for injection molded PET/PE and PC/PE blends

Position	Min. Max. diameter (μm)	Average diameter (μm)
PET/PE blend		
Low injection speed		
G-G section		
Subskin	0.3–1.1	0.8
Intermediate	0.3–1.7	0.9
Core	0.4–3.2	1.2
N-N section		
Subskin	0.3–2.5	1.2
Intermediate	0.3–2.7	1.5
Core	0.4–3.2	1.9
High injection speed		
G-G section		
Subskin	0.3–1.0	0.6
Intermediate	0.3–1.5	0.7
Core	0.3–2.2	1.0
N-N section		
Subskin	0.3–1.8	0.6
Intermediate	0.3–2.1	1.2
Core	0.4–2.9	1.6
PC/PE blend		
Low injection speed		
G-G section		
Subskin	0.2–1.0	0.5
Intermediate	0.3–1.0	0.5
Core	0.3–2.1	0.9
N-N section		
Subskin	0.3–2.1	0.8
Intermediate	0.3–1.2	0.8
Core	0.4–2.0	1.1
High injection speed		
G-G section		
Subskin	0.2–1.0	0.4
Intermediate	0.2–1.2	0.6
Core	0.2–1.2	0.7
N-N section		
Subskin	0.3–1.2	0.5
Intermediate	0.3–1.2	0.6
Core	0.4–1.4	0.8

Therefore, the solidified layer was thinner at the moment of subskin layer formation, and the subskin layer started to develop at a position closer to the surface. This effect also contributed to the subskin layer thickening. In the core zone, as observed in the SEM micrographs, the dispersed domains assumed the form of spheres and ellipsoids regardless of the injection speed. On the other hand, high injection speed brought about strong elongational and shear rate fields to promote the deformation and breakup of the dispersed phase into smaller particles. Besides, the longer cooling time enabled the smaller particles to recover. Therefore the shape of the dispersed particles obtained at high injection speed was close to spherical and their size were smaller than those at low injection speed. However, Ghiam and White [14] observed that the lower the injection rate, the finer is the phase morphology of the injection molded nylon 6/PE blend parts. They argued that the influences of the associated pressure and shear viscosity rise caused by the decrease of injection rate overcome the effect of weaker elongational and shear rate fields.

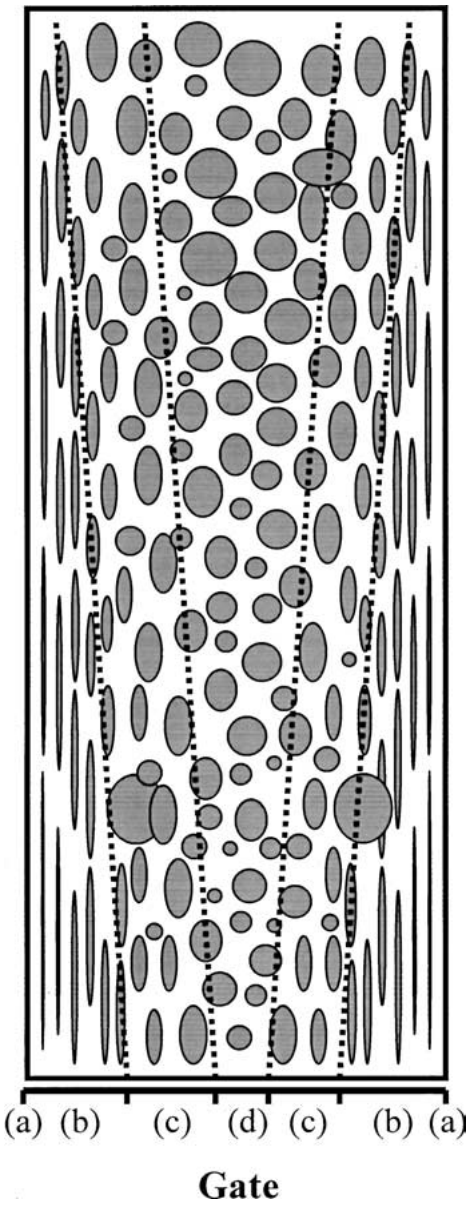

Figure 9 The schematic representation for the morphology of the entire section of the specimen along the melt flow direction: (a) surface, (b) sub-skin layer, (c) intermediate layer and (d) core zone.

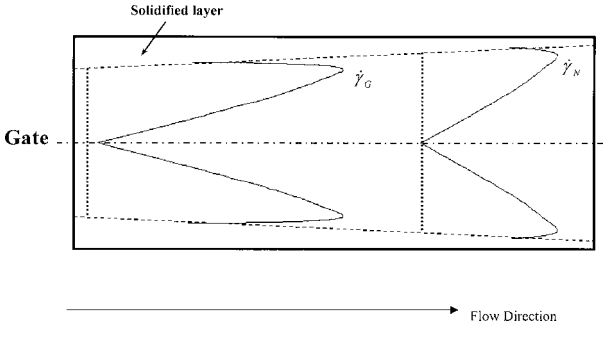

Figure 10 Shear rate profile through the thickness during mold filling near the gate end and the non-gate end.

4. Conclusions

The skin-core structure of injection molded PET/PE and PC/PE blends was investigated by SEM observation using a single-gate mold. The conclusions are as follows:

1. The shape and size of the dispersed PET and PC phases depended not only on the nature properties of PET/PE and PC/PE blends, but also on the injection molding parameters such as injection speed as well as the positions throughout the entire molded bar.

2. The morphology in the section perpendicular to the melt flow direction includes four layers, surface, sub-skin, and intermediate layers as well as core zone. The surface was ignored in the present study. The sub-skin layer contained more or less highly elongated fibers. In the core zone, there were spherical or ellipsoidal particles. Between these two layers, there was an intermediate layer where the dispersed particles mainly assumed the form of fibers, ellipsoids or spheres.

3. Among the four layers, the sub-skin layer has the highest thickness and it decreased gradually along the melt flow direction. Moreover, the diameter of dispersed phase decreased from the gate end toward the non-gate end.

4. The average size of dispersed PET particles was larger than that of PC particles in the blends.

Acknowledgements

The authors gratefully acknowledge the financial support of this work by the Nature Science Foundation of China (grant: 50103007). We are also heavily indebted to Miss Xin-Yuan Zhang and Mr. Zhu Li from Center of Analysis and Test of Sichuan University for careful SEM observation.

References

1. L. M. ROBESON, *Polym. Eng. Sci.* **24** (1984) 587.
2. M. F. BOYAUD, A. AIT-KADI, M. BOUSMINA, A. MICHEL and P. CASSAGNAU, *Polymer* **42** (2001) 6515.
3. Z. M. LI, M. B. YANG, B. H. XIE, J. M. FENG and R. HUANG, *Polym. Eng. Sci.* **41** (2003) 615.
4. J. KARGER-KOCSIS and I. CSIKAI, *ibid.* **27** (1987) 241.
5. C. D. HAN, K. U. KIM, J. PARKER, N. SISKOVIC and C. R. HUANG, *Appl. Polym. Symp.* **20** (1973) 91.
6. R. C. THAMM, *Rubber Chem. Technol.* **50** (1977) 24.
7. W. J. HO and R. SALOVEY, *Polym. Eng. Sci.* **21** (1981) 839.
8. R. E. SKOCHDOPOLE, C. R. FINCH and J. MARSHALL, *ibid.* **27** (1987) 627.
9. B. D. FAVIS, in "Polyemr Blends Vol. 1: Formulation," edited by D. R. Paul and C. D. Bucknall (John Wiley & Sons, New York, 2000) p. 502.
10. B. D. FAVIS and J. P. CHALIFOUX, *Polymer* **29** (1988) 1761.
11. B. D. FAVIS and D. THERRIEN, *ibid.* **32** (1988) 1474.
12. S. Y. HOBBS and V. H. WATKINS, in "Polyemr Blends Vol. 1: Formulation," edited by D. R. Paul and C. D. Bucknall (John Wiley & Sons, New York, 2000) p. 239.
13. L. A. UTRACKI, in "Polymer Alloys and Blends: Thermodynamics and Rheology" (Hanser, Munich, 1989) p. 1.
14. F. GHIAM and J. L. WHITE, *Polym. Eng. Sci.* **31** (1991) 76.
15. S. FELLAHI, B. D. FAVIS and B. FISA, *Polymer* **37** (1996) 2615.
16. Y. SON, K. H. AHN and K. CHAR, *Polym. Eng. Sci.* **40** (2000) 1376.
17. *Idem.*, *ibid.* **40** (2000) 1385.
18. C. M. HSIUNG, M. CAKMAK and Y. ULCER, *Polymer* **37** (1996) 4555.
19. M. N. BUREAU, E. D. FRANCESCO, J. DENAULT and J. I. DICKSON, *Polym. Eng. Sci.* **39** (1999) 1119.
20. J. KARGER-KOCSIS and D. E. MOUZAKIS, *ibid.* **39** (1999) 1365.
21. G. GUERRICA-ECHEVARRIA, J. I. EGUIAZABAL and J. NAZABAL, *J. Appl. Polym. Sci.* **72** (1999) 1113.
22. L. DORAZIO, C. MANCARELLA, E. MARTUSCELLI, G. STICOTTI and G. CEDDHIN, *ibid.* **72** (1999) 701.
23. M. N. BUREAU, H. EI KADI, J. DENAULT and J. I. DICKSON, *Polym. Eng. Sci.* **37** (1997) 377.
24. B. OHLSSON and B. TONELL, *ibid.* **38** (1998) 108.
25. K. W. MCLAUGHLIN, *ibid.* **29** (1989) 1560.
26. M. P. LEE, A. HILTNER and E. BAER, *Polymer* **33** (1992) 675.
27. *Idem.*, *ibid.* **33** (1992) 685.
28. B. FISA, B. D. FAVIS and S. BOURGEOIS, *Polym. Eng. Sci.* **30** (1990) 1051.
29. G. GUERRICA-ECHEVARRIA, J. I. EGUIAZABAL and J. NAZABAL, *Polym. Compos.* **21** (2000) 864.
30. S. K. PAL and D. D. KALE, *J. Polym. Res.* **7** (2000) 107.
31. B. OHLSSON and B. TORNELL, *Polym. Eng. Sci.* **38** (1998) 108.
32. L. DORAZIO and G. CECCHIN, *Polymer* **42** (2001) 2675.
33. B. NYSTEN, A. GHANEM, J. L. COSTA and R. LEGRAS, *Polym. Intern.* **48** (1999) 334.
34. Y. G. SON and K. CHAR, *SPE ANTEC Conf. Proc.* **3** (1996) 2668.
35. Y. D. WANG and M. CAKMAK, *ibid.* **2** (1996) 1581.
36. S. FELLAHI, B. D. FAVIS and B. FISA, *SPE ANTEC Tech. Pap.* **39** (1993) 211.
37. Z. M. LI, W. YANG, B. H. XIE, R. HUANG, M. B. YANG and J. M. FENG, *J. Mater. Sci.* in this issue.
38. K. FRIEDRICH, E. UEDA, H. KAMO, M. EVSTATIEV, B. KRASTEVA and S. FAKIROV, *J. Mater. Sci.* **37** (2002) 4299.
39. K. MIN, J. L. WHITE and J. F. FELLERS, *Polym. Eng. Sci.* **24** (1984) 1327.
40. J. R. STELL, D. R. PAUL and J. W. BARLOW, *ibid.* **16** (1976) 496.
41. M. V. TSEBRENKO, *Intern. J. Polym. Mater.* **10** (1983) 83.
42. N. CHAPLEAU and B. D. FAVIS, *J. Mater. Sci.* **30** (1995) 142.
43. R. G. COX, *J. Fluid Mech.* **37** (1969) 601.
44. D. I. TAYLOR, *Proc. Royal Soc.* **A146** (1934) 501.
45. R. GONZALEA-NUNEZ, C. F. CHAN MAN FONG, B. D. FAVIS and D. D. KEE, *J. Appl. Polym. Sci.* **62** (1996) 1627.
46. C. V. D. REIGDEN-STOLK and A. SARA, *Polym. Eng. Sci.* **26** (1986) 1229.
47. J. J. ELMENDORP, *ibid.* **26** (1986) 418.

Received 18 July
and accepted 14 August 2003